Limnological conditions in Subglacial Lake Vostok, Antarctica

Brent C. Christner[1]
Department of Land Resources and Environmental Sciences, 334 Leon Johnson Hall, Montana State University, Bozeman, Montana 59717

George Royston-Bishop
Bristol Glaciology Centre, School of Geographical Sciences, University of Bristol, Bristol BS8 1SS, United Kingdom

Christine M. Foreman
Department of Land Resources and Environmental Sciences, 334 Leon Johnson Hall, Montana State University, Bozeman, Montana, 59717; Center for Biofilm Engineering, 366 EPS Building, Montana State University, Bozeman, Montana 59717

Brianna R. Arnold
Department of Land Resources and Environmental Sciences, 334 Leon Johnson Hall, Montana State University, Bozeman, Montana 59717

Martyn Tranter
Bristol Glaciology Centre, School of Geographical Sciences, University of Bristol, Bristol BS8 1SS, United Kingdom

Kathleen A. Welch and W. Berry Lyons
Byrd Polar Research Center, Department of Geological Sciences, The Ohio State University, 1090 Carmack Road, Columbus, Ohio 43210-1002

Alexandre I. Tsapin
Astrobiology Group, Jet Propulsion Laboratory, California Institute of Technology, 4800 Oak Grove Drive, MS 183-301, Pasadena, California 91109-8099

Michael Studinger
Lamont-Doherty Earth Observatory of Columbia University, 61 Route 9W, Palisades, New York 10964-8000

John C. Priscu[2]
Department of Land Resources and Environmental Sciences, 334 Leon Johnson Hall, Montana State University, Bozeman, Montana 59717

Abstract

Subglacial Lake Vostok is located ~4 km beneath the surface of the East Antarctic Ice Sheet and has been isolated from the atmosphere for >15 million yr. Concerns for environmental protection have prevented direct sampling of the lake water thus far. However, an ice core has been retrieved from above the lake in which the bottom ~85 m represents lake water that has accreted (i.e., frozen) to the bottom of the ice sheet. We measured selected constituents within the accretion ice core to predict geomicrobiological conditions within the surface

---

[1] Present address: Department of Biological Sciences, 202 Life Sciences Building, Louisiana State University, Baton Rouge, Louisiana 70803.

[2] Corresponding author (jpriscu@montana.edu).

waters of the lake. Bacterial density is two- to sevenfold higher in accretion ice than the overlying glacial ice, implying that Lake Vostok is a source of bacterial carbon beneath the ice sheet. Phylogenetic analysis of amplified small subunit ribosomal ribonucleic acid (rRNA) gene sequences in accretion ice formed over a deep portion of the lake revealed phylotypes that classify within the β-, γ-, and δ-*Proteobacteria*. Cellular, major ion, and dissolved organic carbon levels all decreased with depth in the accretion ice (depth is a proxy for increasing distance from the shoreline), implying a greater potential for biological activity in the shallow shoreline waters of the lake. Although the exact nature of the biology within Lake Vostok awaits direct sampling of the lake water, our data from the accretion ice support the working hypothesis that a sustained microbial ecosystem is present in this subglacial lake environment, despite high pressure, constant cold, low nutrient input, potentially high oxygen concentrations, and an absence of sunlight.

Lake Vostok is the largest of more than 140 subglacial lakes that have been identified (Priscu et al. 2003; Siegert et al. 2005) and is one of the largest lakes on Earth, with a surface area and volume of 14,000 km^2 and ~5,400 km^3, respectively (Studinger et al. 2004; Siegert et al. 2005). Despite extremely cold air temperatures above the ice (average = $-55°C$; National Climatic Data Center, http://www.ncdc.noaa.gov/oa/ncdc.html), liquid water is stable in the lake owing to the combined effect of background geothermal heating, the insulating properties of the overlying ice sheet, and adiabatic lowering of the freezing point (Siegert et al. 2003).

The site selection for Vostok Station (Fig. 1) by the Soviet Antarctic Expedition in 1957 was fortuitous for subglacial lake research because it was originally chosen to collect ice cores for paleoclimate reconstruction (e.g., Petit et al. 1999). Several ice cores have been recovered from the ice sheet at Vostok Station since the mid-1960s, the deepest of which was the result of a coordinated Russian, French, and American effort that removed 3,623 m of ice core (designated borehole 5G). Drilling was terminated in 1998 in a zone of accretion ice ~120 m above the water–ice interface owing to concerns of contaminating the pristine lake environment below (e.g., Inman 2005), which might have been isolated from direct contact with the atmosphere for at least 15 million yr (Siegert et al. 2003). A solely Russian drilling effort began again in 2006 with the removal of an additional 27 m of ice core (3,624–3,651 m; V. Lukin pers. comm.). The Russian Antarctic Expedition plans to mechanically drill another ~75 m and then penetrate the lake with a thermal drill, which is scheduled to occur within 3 yr (Inman 2005).

The upper 3,309 m of the Vostok 5G ice core is of meteoric origin and provides a detailed paleoclimate record spanning the past 420,000 yr (Petit et al. 1999). Ice at depths between 3,310 and 3,539 m is also of meteoric origin but has been extensively deformed by contact with bedrock and, therefore, does not contain interpretable paleoclimate data (Petit et al. 1999). The basal portion of the ice core from 3,539 to 3,623 m (Fig. 1C) has a chemistry and crystallography distinctly different from the overlying glacial ice, including extremely low electrical conductivity, large ice crystals (Jouzel et al. 1999), and numerous macroscopically visible sediment inclusions (Simões et al. 2002; Souchez et al. 2002; Royston-Bishop et al. 2005). The geochemical composition of this basal ice, in concert with the geophysical data, indicates that the basal portion of the core represents actual lake water that has accreted (i.e., frozen) to the underside of the ice sheet. The ice sheet flow path (Fig. 1B) indicates that accretion ice between 3,539 and 3,609 m (type I accretion ice) formed from lake water that accreted in a shallow embayment in the southwestern portion of the lake (Bell et al. 2002), whereas accretion ice between 3,610 and 3,623 m (type II accretion ice) is much cleaner and formed over the deep central portion of the lake's southern basin (de Angelis et al. 2004). Thus, ice recovered at increasing depth within the accretion zone represents a transect of frozen surface waters from Lake Vostok as the ice sheet flowed from a shallow embayment in the west to the open lake water in the east (Bell et al. 2002).

The freshwater in Lake Vostok originates from the overlying ice sheet, which melts near the shoreline of the lake and at the ice–water interface in the northern portion of the lake (Siegert et al. 2000; Studinger et al. 2004). Accretion to the base of the ice sheet occurs in the central and southern regions (i.e., within the shallow embayment; Bell et al. 2002) and continues as the ice flows into deeper water (Fig. 1B), removing water from the lake (Siegert et al. 2000). The accretion ice is essentially gas-free relative to the overlying glacial ice (Jouzel et al. 1999), leading to high dissolved gas levels (2.5 L kg^{-1} water; McKay et al. 2003) supplied from air hydrates released as glacial ice melts into the lake. The dissolved oxygen concentration has been predicted to be ~50 times higher than air-equilibrated water and much of it is thought to exist as air hydrates within the water column (McKay et al. 2003). Although these oxygen estimates assume no biogenic alteration within the lake, it has been hypothesized that aerobic conditions in the upper portion of the water column could support autotrophic and heterotrophic metabolic lifestyles, whereas deeper portions of the lake and sediment are likely to be anoxic if biotic and abiotic O$_2$ sinks

Fig. 1. (A) Composite RADARSAT synthetic aperture image of the ice above subglacial Lake Vostok (data available from the National Snow and Ice Data Center, http://nsidc.org/). Contour lines are ice surface elevation (10-m interval) from airborne laser altimetry (Studinger et al. 2003). The lake shows as the flat featureless region in the center of the image. White box marks map area shown in (B), the southern shoreline of Lake Vostok. Solid white lines mark airborne radar echo profiles with lake reflections (Studinger et al. 2003). The flow line through the Vostok ice core (black dashed line) has been derived by tracking internal structures in the ice over the lake and the gradient of the ice surface over grounded ice (Bell et al. 2002). (C) Airborne ice-penetrating radar profile through the Vostok 5G core site. Eighty-five meters of accretion ice was drilled at 5G in 1998 and an additional 27 m was recovered during the 2005–2006 austral summer (V. Lukin pers. comm.).

exist (Siegert et al. 2003). The heterotrophic potential of the lake is supported by measurable dissolved organic carbon concentrations in the accretion ice (Karl et al. 1999; Priscu et al. 1999), together with microbial respiration of organic substrate in melted ice samples (Karl et al. 1999).

Geothermal energy input into the lake from high-enthalpy mantle processes or seismotectonic activity (Bulat et al. 2004) has been speculated, although a ^{3}He : ^{4}He signature typical of an old continental province in the accretion ice rules out the former (Jean-Baptiste et al. 2001). The increased He concentration and lower ^{3}He : ^{4}He ratio in the accretion ice compared with glacial ice imply these signatures could equally originate from the subglacial comminution of rock. Bulat et al. (2004) suggested that fault activity could sustain thermophilic chemolithoautotrophic microbial communities, a notion consistent with thermophile-related small subunit rRNA gene sequences found in accretion ice samples (Christner et al. 2001; Bulat et al. 2004), and minor tectonic activity detected near the Lake Vostok basin (Studinger et al. 2003) which could introduce significant amounts of thermal energy. If this emerging picture is correct, the deep waters of Lake Vostok could harbor an ecosystem fueled by geochemical energy, much like that observed in deep-sea hydrothermal vent systems.

Microbiological and molecular-based studies of the accretion ice have shown low but detectable amounts of prokaryotic cells and deoxyribonucleic acid (DNA; Karl et al. 1999; Priscu et al. 1999; Christner et al. 2001). Metabolic and culture experiments demonstrated that a portion of the assemblage in the accretion ice is metabolically active when exposed to liquid water and organic electron donors (Karl et al. 1999; Christner et al. 2001). Molecular identification of microbes within the accretion ice (by culturing and small subunit rRNA gene amplification) show close agreement with present day surface microbiota that classify within the bacterial phyla *Proteobacteria* (α, β, and γ), *Firmicutes*, *Actinobacteria*, and *Bacteroidetes* (Priscu et al. 1999; Christner et al. 2001; Bulat et al. 2004). All of the studies described above focused on a limited number of accretion ice sections, most of which formed in the shallow western embayment, and therefore do not reveal the limnological nature of the system.

Here we present results from an extensive microbiological and geochemical study of ice recovered from the Vostok 5G borehole. Many horizons of both glacial and accretion ice were analyzed to estimate the biogeochemical and microbiological conditions in the lake. We discuss the implications of this new comprehensive data set for discerning plausible ecological scenarios for microbial life in Subglacial Lake Vostok. Our data will allow scientists to design meaningful experiments when the lake is eventually sampled, which should be within the next few years (Inman 2005).

Materials and methods

Site description—Vostok Station (78°27′S, 106°52′E; Fig. 1) is located near the center of the East Antarctic Ice Sheet. The first evidence for the existence of a large lake beneath Vostok Station came from radio echo sounding profiles (Robin et al. 1977) and ERS-1 radar altimeter data (Ridley et al. 1993), which both revealed a strikingly flat surface above the lake. Aerogeophysical measurements indicate that Lake Vostok has a surface area >14,000 km² (Kapista et al. 1996) and a volume of 5,400 ± 1,600 km³ (Studinger et al. 2004). The lake consists of a smaller northern basin (~500 m deep) and deeper (~800 m) southern basin, separated by a sill of ~200 m (Studinger et al. 2004). The overlying glacial ice is ~4,200 m thick over the northern basin, thinning to ~3,900 m over the southern portion of the lake (Kapista et al. 1996). The difference in ice thickness produces a gradient in the pressure freezing point (Kapista et al. 1996), which would drive water circulation (Wüest and Carmack 2000; Siegert et al. 2003). The surface waters will be at the pressure melting point of -2.5 to $-2.8°C$ (Wüest and Carmack 2000), and total dissolved solids have been predicted to range from ~1 to 40 mmol L^{-1} (Priscu et al. 1999; Siegert et al. 2003; Royston-Bishop et al. unpubl. data).

Ice core description—Detailed information on the depth, age, and quantities of ice samples examined in this study is presented in Table 1. Ice cores from 171 to 3,605 m were obtained from the U.S. National Ice Core Laboratory (Denver, Colorado), and cores from 3,612 and 3,622 m were obtained from the Laboratoire de Glaciologie et Géophysique de l'Environnement (Grenoble, France). Embedded data loggers indicated that the temperature from collection to receipt of the ice never exceeded $-15°C$. Ice cores were stored in sealed polyethylene tubing at $-25°C$ and archived in a subzero research facility at Montana State University during all phases of our study.

Ice core sampling—Ice cores were sampled according to the decontamination protocol described by Christner et al. (2005). Briefly, ice cores were intentionally contaminated with a 15% (v/v) glycerol mixture containing *Serratia marcescens*, a target DNA sequence (plasmid), and the fluorescent dye rhodamine 6G. Samples removed sequentially from the core exterior were tested for the presence of the introduced contamination by cultivation, direct cell counting, the polymerase chain reaction (PCR), and fluorometric analysis. After the tracer mixture was applied, the exterior portion (5 mm of the radius; 10 mm of the diameter) of the ice core was physically removed by scraping with a sterile microtome blade to remove the contaminated exterior of the sample and expose previously unhandled ice. The scraped ice samples were thoroughly washed with 95% ethanol and then rinsed with sterile deionized H_2O within a Class 100 Purifier Horizontal Clean Bench (Labconco Corporation, model 36125) to disinfect and remove another ~5-mm layer of the ice core. The ice core was incubated at 22°C in a sterile glove box purged

and filled with 0.2-μm–filtered zero-grade air until at least 15 mm of the original core radius had melted. The remaining ice was sealed within a sterile container and allowed to melt completely in the dark at 0–4°C, which required at least 72 h. The migration of the kerosene-based drilling fluid into the core was analyzed for selected samples by gas chromatography–mass spectrometry and shown to be negligible following the protocol described above (Christner et al. 2005).

Our sampling protocol eliminated cells, nucleic acids, and drilling fluid contaminants associated with the ice cores after ≥1.5 cm of the core exterior (i.e., 3 cm of the diameter) was removed (Christner et al. 2005). A "control" blank ice core constructed and analyzed in parallel with 5G ice core samples indicated that background particulate matter contamination represented fewer than 10 particulates >1 μm per field of view, which was <20% of the lowest concentration of particulates observed in any of the samples. The decontamination protocol, which was performed on each core sampled, provided uncompromised meltwater for all of the analyses presented in this report.

Cell enumeration and viability assessment—A 10-mL sample of the meltwater was fixed in 5% formalin and stained with SYBR Gold™ for 15 min as outlined in Lisle and Priscu (2004) The sample was filtered onto a 5-mm spot of a 25-mm diameter, 0.2-μm pore size black polycarbonate filter (Poretics, cat. No. K02BP02500) with a dot blot apparatus and vacuum (25 kPa). Filters were mounted on glass microscope slides with the addition of two drops of an antifade solution, which consisted of 0.1% *p*-phenylenediamine (Sigma, cat. No. P-1519) in a 1:1 (weight : volume) solution of phosphate-buffered saline and glycerol. All filtering and manipulations were conducted within a BioGard vertical laminar flow hood that eliminates 99.99% of atmospheric particles <0.3 μm (Baker Company, model B6000-1) equipped with a germicidal ultraviolet (UV)-C lamp. The reagents used for DNA staining (i.e., sodium borate–buffered formalin [37% formaldehyde] and SYBR Gold [Molecular Probes, cat. No. S-11494]) were passed through 0.2-μm filters to remove extraneous particles and cells before use. The LIVE/DEAD® BacLight™ Bacterial Viability Kit (Molecular Probes, cat. No. L7007) was used to differentially stain live and dead cells on the basis of the integrity of the plasma membrane. A 10-mL sample was filtered as described for total cell density (i.e., SYBR Gold staining), except filtration and all manipulations were done at <4°C. The filter was covered with 200 μL of a solution containing 6 μmol L^{-1} SYTO 9 stain and 30 μmol L^{-1} propidium iodide and incubated for 15 min in the dark. The solution was vacuum filtered (25 kPa), and the filters were mounted on glass microscope slides and visualized with low-fluorescence immersion oil.

Cells on the filters were counted with a Nikon Optiphot epifluorescent microscope equipped with a DM510 filter cube (Nikon) at a final magnification of ×1,000. The total number of cocci and rods in 60 fields of view (one field of view at ×1,000 = 16,741 μm²) was determined and the number of cells per milliliter of ice core meltwater was

Table 1. Depth (meters below the ice sheet surface), origin, age, and mass of Vostok ice core samples examined.

Core ID*	Core age ($\times 10^3$ yr B.P.) †	Top depth (m)	Bottom depth (m)	Mass collected (g of ice) ‡
171§	6.72	170.24	170.74	580
179§	7.12	178.00	179.00	1,110
763	50.5	762.00	762.32	1,000
1,577	114	1,576.00	1,576.33	1,000
1,686	114	1,685.27	1,685.77	700
2,091	121	2,090.30	2,090.60	650
2,303	178	2,302.00	2,302.50	530
2,334	182	2,333.50	2,334.00	700
2,490	202	2,489.00	2,489.31	625
2,749	237	2,748.43	2,748.94	630
2,758	238	2,758.42	2,758.49	210
3,015	298	3,014.71	3,015.00	580
3,081	315	3,080.70	3,080.73	100
3,197	360	3,196.28	3,196.51	580
3,351‖	>420	3,350.05	3,350.50	500
3,519‖	>420	3,518.03	3,518.44	300
3,537‖	>420	3,536.50	3,536.68	210
3,540¶	5.1	3,539.62	3,539.99	350
3,548¶	4.9	3,547.00	3,547.50	330
3,566¶	4.4	3,564.99	3,565.32	360
3,567¶	4.4	3,566.57	3,566.76	287
3,569¶	4.4	3,568.10	3,568.32	284
3,570¶	4.3	3,569.60	3,569.77	291
3,572¶	4.3	3,571.16	3,571.38	300
3,573¶	4.3	3,572.44	3,572.74	492
3,575¶	4.2	3,574.06	3,574.23	301
3,576¶	4.2	3,575.70	3,575.86	285
3,578¶	4.1	3,577.12	3,577.30	273
3,579¶	4.1	3,578.50	3,578.68	293
3,581¶	4.1	3,580.27	3,580.41	247
3,582¶	4.0	3,581.80	3,582.00	282
3,585¶	4.0	3,584.66	3,584.83	205
3,588¶	3.9	3,587.15	3,587.45	303
3,591¶	3.8	3,590.75	3,590.88	187
3,605¶	3.5	3,604.01	3,604.49	505
3,612¶	3.3	3,611.00	3,611.34	490
3,622¶	3.0	3,621.00	3,621.58	810

* Ice core samples are designated by the depth of recovery from below the surface. Core ID represents tube number and approximate depth in meters below the surface.

† Dates for samples 171–3,197 are based on the time scale of Petit et al. (1999). For samples 3,540–3,622, the age since accretion on the basis of an approximate accretion rate of ~4 cm yr^{-1} (Bell et al. 2002) and a total accretion ice thickness of 3,743 m.

‡ Amount of sample available for analysis after implementing decontamination protocols (Christner et al. 2005).

§ Ice cores from the BH5 borehole: 179-m dry core drilled in 1991–1992. All others from 5G borehole: 3,623-m core drilled with kerosene/freon fluid mixture in 1991–1997.

‖ Ice from deformed layer; no interpretable paleoclimatic record, but of meteoric origin and older than deepest dated section (4.20×10^5 yr B.P.; Petit et al. 1999).

¶ Ice core samples not of meteoric origin (i.e., derived by accretion of water from Lake Vostok onto the bottom of the ice sheet; Jouzel et al. 1999).

calculated according to the procedure outlined by Lisle and Priscu (2004). Procedural blanks treated in a manner identical to the samples indicated that cellular contamination associated with collection, staining, and filtering was always <20 cells mL^{-1} and was ≤5 cell mL^{-1} for most (60%) of the samples analyzed.

Respiration and incorporation of [^{14}C]glucose—Ice core meltwater (55 mL) was combined with 44 μL of [U-^{14}C]-D-glucose (370 MBq mmol^{-1}; MP Biomedicals, cat. No. 0111049.2, lot No. 6361150) in a sterile 100-mL polycarbonate bottle yielding a final concentration of 80 μmol L^{-1} and a final activity of 1.8×10^6 disintegra-

tions min^{-1} mL^{-1}. Aliquots (5 mL) were transferred into stoppered 25-mL ''respiration'' vials (Kontes, cat. No. K882360-0025) equipped with a basket containing a folded GF/F filter (Whatman, cat. No. 1825-025) suspended above the aqueous phase. The respiration vials were autoclaved before the filter basket, and septa were installed and microwaved at 1,000 W for 2 min after addition of the septa and basket containing the filter. All experimental manipulations were conducted in a BioGard vertical laminar flow hood with a germicidal UV-C lamp, and solutions and sample vials were maintained on ice at <4°C. Each experiment had five kills, which were treated identically to the live samples (six replicates), except that

meltwater was transferred directly into a respiration vial that contained 1 mL of 25% ice cold trichloroacetic acid (TCA). All samples were incubated for 19–20 d at 10°C in the dark. After incubation, the reaction in the nonkilled samples was terminated by the addition of 1 mL of 25% ice cold TCA (final concentration 5%). The TCA precipitated macromolecules and lowered the pH of the sample to <2, converting all inorganic carbon to CO_2. β-Phenethylamine (0.1 mL; Sigma, cat. No. P 2641) was added to the GF/F filter through a septum with a sterile syringe and needle to trap respired CO_2. Samples were then maintained at 4°C for 24 h with gentle swirling (~30 rpm) to ensure that all CO_2 was trapped on the treated wick (preliminary time course experiments showed that this protocol trapped all $^{14}CO_2$ in the headspace). The liquid phase was filtered through a 0.2-μm polycarbonate filter (Poretics, cat. No. K02CP02500), and the sample vial and towers were rinsed with 6 mL of ice cold 5% TCA (three 2-mL rinses). Filters (0.2-μm polycarbonate and the β-phenethylamine–amended GF/F filters) were placed in 20-mL scintillation vials containing 20 mL of Cytoscint™ ES scintillation cocktail (MP Biomedicals, cat. No. 882453), and the radioactivity was quantified by standard liquid spectrometry. Vials containing only 0.1 mL of β-phenethylamine and the scintillation cocktail were included to monitor and correct for potential chemiluminescence.

PCR amplification, cloning, and sequencing of small subunit rRNA gene sequences—The possibility of erroneous PCR amplification was a primary concern in these experiments; therefore, stringent precautions were taken to clarify reagents and workspaces of nucleic acid contamination and verify the authenticity of results obtained. All manipulations were conducted within a Bio-Gard vertical laminar flow hood that was thoroughly cleaned with a solution of 0.5% (w/v) sodium hypochlorite. Autoclaved and ethylene-oxide–sterilized (105 min at 600 mg L^{-1}, 60% relative humidity at 30°C) materials (0.2-μm–filtered water, pipettes, tubes, hydrophobic-barrier pipette tips, and test tube racks) were placed in the hood and exposed to DNA-damaging UV-C radiation for at least 30 min before all experiments. A two-stage nested PCR strategy (e.g., Priscu et al. 1999) was used to amplify a portion of the small subunit rRNA gene sequence directly from the ice core meltwater. The optimal annealing temperature for each primer set was determined in separate experiments with the use of genomic DNA from known bacteria and by conducting PCR amplifications over a 15°C temperature annealing gradient (45–60°C). For the first round of amplification, the 100-μL reaction mixture contained 67.5 μL of distilled water (dH$_2$O) plus ice core meltwater (i.e., 67.5 μL of sample or 10 μL sample + 57.5 μL dH$_2$O), 10 μL of the 10× reaction buffer provided by the manufacturer, 200 μmol L^{-1} of each nucleotide (2′-deoxyadenosine 5′-triphosphate [dATP], 2′-deoxycytidine 5′-triphosphate [dCTP], 2′-deoxyguanosine 5′-triphosphate [dGTP], 2′-deoxythymidine 5′-triphosphate [dTTP]), 0.2 μmol L^{-1} of the forward primer 27F (*Escherichia coli* numbering) and reverse primers 1492R or 1525R (Lane 1991), 4 mmol L^{-1} MgCl$_2$, and 2.5 U of AmpliTaq Gold

DNA polymerase, LD (Applied Biosystems, cat. No. 4338856). The AmpliTaq Gold DNA polymerase is a chemically modified, heat-activated enzyme that is stringently purified to reduce background levels of contaminating bacterial DNA (Applied Biosystems, product informational insert). All components of the PCR mixture, except for the AmpliTaq Gold DNA polymerase, were passed through Microcon YM-100 filters (Millipore, cat. No. 4211) to remove contaminating double-stranded nucleic acids with >125 nucleotides. Samples were incubated at 95°C for 5 min in an Eppendorf Mastercycler Gradient Thermal Cycler and then amplified for 25 cycles by denaturing for 15 s at 95°C, annealing for 15 s at 50°C, and extension for 90 s at 72°C. A final extension for 7 min at 72°C was conducted at the end of the amplification cycle. An aliquot (1 μL) of the resulting product was used as the template in the second PCR amplification, with the forward primer 515F combined with the reverse primers 926R, 1392R, or 1492R (Lane 1991; Reysenbach and Pace 1995). The conditions for amplification were identical to the first round, except that the reaction volume was reduced to 50 μL, and 30 cycles of amplification were used. For each individual amplification experiment, three negative controls from the master mix used to construct the amplification reactions for the actual samples were analyzed in parallel. In addition, these PCR analyses included amplification reactions targeting a plasmid DNA sequence intentionally contaminated on the ice core surface before sampling, with the use of primers and amplification conditions described by Christner et al. (2005). Samples from each PCR reaction were evaluated by electrophoresis through a 1% agarose gel followed by staining with ethidium bromide.

Individual DNA molecules were cloned from the 400–1,000 base pair populations into the pGEM-Teasy vector (Promega, cat. No. A1380), and ~25 clones with inserts of the predicted size in each library were screened for sequence diversity by restriction fragment length polymorphism with the restriction enzymes *Hin*PI and *Msp*I (New England Biolabs, cat. nos. R0124S and R0106S, respectively). Clones with unique inserts were bidirectionally sequenced with primers that annealed the flanking T7 and SP6 universal promoter sequences. The amplified sequences were checked for chimeras with the Ribosomal Database Project II Chimera Check (http://wdcm.nig.ac.jp/RDP/html/index.html) and Bellerophon Server (http://foo.maths.uq.edu.au/~huber/bellerophon.pl), manually evaluated for covariance, and aligned on the basis of positional homology for phylogenetic analysis by the ARB software package (Ludwig et al. 2004) and the beta-4b10 version of PAUP 4.0 (Swofford 1999).

Nonpurgeable organic carbon and major ion concentration measurements—Samples for nonpurgeable organic carbon (NPOC) analyses were prepared according to Christner et al. (2005) and measured on a Shimadzu TOC-5000A. NPOC is the dissolved and particulate organic carbon remaining in samples on acidification with 2 mol L^{-1} HCl and sparging for 7 min. All glassware used in the analyses was soaked overnight in NoChromix acid solution (GODAX Laboratories), followed by six rinses

with nanopure water and 8 h of baking at 500°C. Standards were mixed from National Institute of Standards and Technology traceable potassium hydrogen phthalate in nanopure water and were run in conjunction with low total organic carbon consensus reference samples. Six replicate injections were made of acidified and sparged samples. Blanks consisted of acidified and sparged nanopure water. Precision for NPOC measurements was determined by running four of the hydrogen phthalate standards nine times. The precision, calculated as the coefficient of variation, $100s/\bar{x}$ (where s is standard deviation and $\bar{x}$ is the mean), of the concentrations in the replicates, was <12%. The detection limit was ~10 ppb (Priscu et al. 1999).

For other geochemical measurements, samples of ice cores were cut with a band saw at −10°C and lightly scraped (at least 0.5 mm from each surface) with a clean razor blade to remove any possible contamination and condensation frozen onto the surface. Samples that had surface imperfections caused by the ice core drilling rig were more thoroughly scraped to remove any potential contamination in the grooves. The razor blade was cleaned with a dry Kimwipe™ between samples. Only a clean latex glove touched the ice and new gloves were worn for each sample during scraping.

Ice samples were transferred to a BioGard laminar flow hood and allowed to warm to room temperature (~20°C) until the surface began to melt (~5 min). The ice was then held with clean stainless steel forceps and rinsed thoroughly with ~300 mL of 0.2-μm–filtered nanopure water. The rinsed ice was then placed in a new Ziplok® freezer bag that had been rinsed three times with 0.2-μm–filtered nanopure water and allowed to melt completely (~3 h) at room temperature. Samples for major ions were collected from the bags with plastic pipettes and transferred to clean 60-mL high-density polyethylene (HDPE) bottles and stored frozen at −20°C until analysis. The HDPE bottles were cleaned by rinsing twice with 0.2-μm–filtered nanopure water, filled and soaked for 24 h, then rinsed three times immediately before use.

Major ion concentrations were determined with a Dionex DX-120 chromatography system (Welch et al. 1996). The eluent flow rate was 1.2 mL min^{-1} for both anion and cation analysis, and the sample loop was approximately 400 μL for all samples and standards. Cation analysis employed a Dionex IonPac CS12A analytical column (4 × 250 mm) and a CG12A guard column (4 × 50 mm). The eluent was 0.13% methanesulfonic acid solution. A Cation Self-Regenerating Suppressor (CSRS-Ultra; Dionex) was used. Anion analysis employed a Dionex IonPac AS14 analytical column (4 × 250 mm) and an AG14 guard column (4 × 50 mm). The eluent was a 1.0 mmol L^{-1} NaHCO$_3$ and 3.5 mmol L^{-1} Na$_2$CO$_3$ solution. Precision, calculated as the coefficient of variation, for major ion concentrations was <10% for all ions, except for K$^+$, for which precision approached 20%. Accuracy, calculated as the relative mean error with respect to known standards, ranged from 0.0% to 22.3%.

A control ice core was prepared by freezing nanopure water in a clean polycarbonate tube to examine the level of particle and geochemical contamination caused by ice core handling. This core was treated in exactly the same way as the Vostok 5G ice core samples. The nanopure water used for cleaning apparatuses and final rinses from the Ziplok bags were also collected in a HDPE bottle for analysis.

Scanning electron microscopy, particle counts, and mineralogy—Samples were taken from the Ziplok bags (described above) with clean polycarbonate pipettes, placed in 50-mL Falcon™ tubes, and stored at 4°C until filtration. Ten milliliters of each sample was vacuum filtered (25 kPa) onto a 5.0-mm spot of a 0.2-μm Au-Pd–coated polycarbonate filter (Poretics, cat. No. K02CP02500; coating thickness = 15 nm) with a dot-blot filtration system. After filtration, the system was carefully disassembled, and the filter was sealed in a clean glass petri dish. The 5.0-mm spot of the filter was cut out with a clean razor bade and mounted on an aluminum scanning electron microscope (SEM) stub containing electrically conductive tabs. The filter was then sputter coated with carbon to a thickness of 15 nm. Filtration and sample mounting occurred under the BioGard laminar flow hood. For each of five randomly selected fields of view, pairs of secondary electron images (SEI) and backscattered electron images (BEI) were collected at ×500 magnification (JEOL 6100 SEM, accelerating voltage = 15 kV). Particles >1 μm on the images were sized, traced, and counted by SigmaScan Pro 5™ software (SPSS Inc.). The surface area and volume of each particle was estimated by assuming they were spherical with a diameter equal to the longest axis. Energy-dispersive spectrometry (EDS) was used to determine the elemental composition of particles >1 μm on each filter. X-rays were integrated for 40 s to produce clear elemental peaks in the x-ray spectrum. Mineral character was determined on 88 particles from glacial ice and 75 particles from accretion ice, respectively. Procedural blanks (i.e., samples of the control ice core and Barnstead nanopure water) were analyzed to determine the level of background contamination associated with the sampling procedure.

Secondary electron images and BEI were used in concert to differentiate mineral from organic particles on the basis of their density. Organic particles are only visible on the SEI, whereas mineral particles are visible on both the SEI and the BEI. The efficacy of this method was verified with EDS data for more than 40 particulates. In total, the mineral or organic nature of 1,603 particles in Vostok glacial ice and 727 in the accretion ice was determined. The percentage of particulate organic matter in each sample (Table 2) was computed on both a volumetric and numerical basis.

Extraction and quantification of amino acids—Ice melt (1 mL) was placed in a clean screw-cap tube and dried with a SpeedVac (Savant). One milliliter of 6 mol L^{-1} HCl was added to each dried sample and incubated at 100°C for 16 h. The acidified samples were then dried and resuspended in 50 μL of nanopure water. HCl-extractable amino acids (i.e., protein + dissolved combined amino acids [DCAAs] + dissolved free amino acids [DFAAs]; Rosenstock and Simon

Table 2. The proportion of particulate organic matter in selected depths of ice from the Vostok 5G core.

Depth (m)	% organic by volume	% organic by number
1,686	59	38
2,303	52	31
2,334	23	15
2,758	62	39
2,779	88	26
3,081	49	22
3,334	93	22
3,537	36	40
3,548	36	32
3,572	80	58
3,605	67	62
3,610	75	33

2001) were measured in this solution by high-pressure liquid chromatography (HPLC) separation of fluorescent diastereomeric derivatives. Desalted extracts were derivatized with *o*-phthaldialdehyde/*N*-acetyl-L-cysteine, and the derivatives were separated and identified by reversed-phase HPLC on a C18 column (Phenomenex) with 50 mmol L^{-1} sodium acetate and methanol as the solvent. Eluted amino acid derivatives were detected with a fluorescence detector, with $\lambda_{excitation}$ = 340 nm and $\lambda_{emission}$ = 450 nm.

Results and discussion

Cells and particles—The density of SYBR Gold–stained cells in the glacial ice above Lake Vostok (sampled at 15 depths between 171 and 3,537 m; Fig. 2A) ranged from 34 ± 10 to 380 ± 53 cells mL^{-1} (mean ± standard deviation) of ice core meltwater, and the concentration of total particles >1 μm ranged from 4,000 to 12,000 cells mL^{-1} (Fig. 2B). Cell density in the deepest portion of the glacial ice (3,519 and 3,537 m) was among the lowest observed in the entire 5G profile (54 ± 12 and 59 ± 19 SYBR Gold–stained cells mL^{-1}, 94 ± 17 and 98 ± 31 total BacLight-stained cells mL^{-1}, respectively; Fig. 2B). Although the glacial ice at this transition represents the deepest ice of meteoric origin, it is unlikely to have been in direct contact with bedrock because as the ice flows across the lake, the base of the ice sheet melts for the first ~8 km before accretion starts (Siegert et al. 2000). This contention is supported by the low mass and size of particles in this portion of the core (Fig. 2B) compared with other ice cores that have reached bedrock. For example, the basal debris in GISP2 (central Greenland) and Byrd ice cores (Antarctica) comprises 0.3–15% of the total weight of the ice and contains individual particles that can reach 2 cm in diameter (Gow and Meese 1996) compared with maximum values of ~0.00009% by weight and 70 μm maximum size in the Vostok ice core, respectively (Simões et al. 2002; Royston-Bishop et al. 2005). Furthermore, refrozen basal ice from polar ice sheets and glaciers typically contains significantly higher cell concentrations than those in the overlying glacial ice (e.g., Sharp et al. 1999; Sheridan et al. 2003).

Given the high degree of spatial heterogeneity in physical and chemical parameters (e.g., grain boundaries and sediment inclusions) in ice from the Vostok core (Souchez
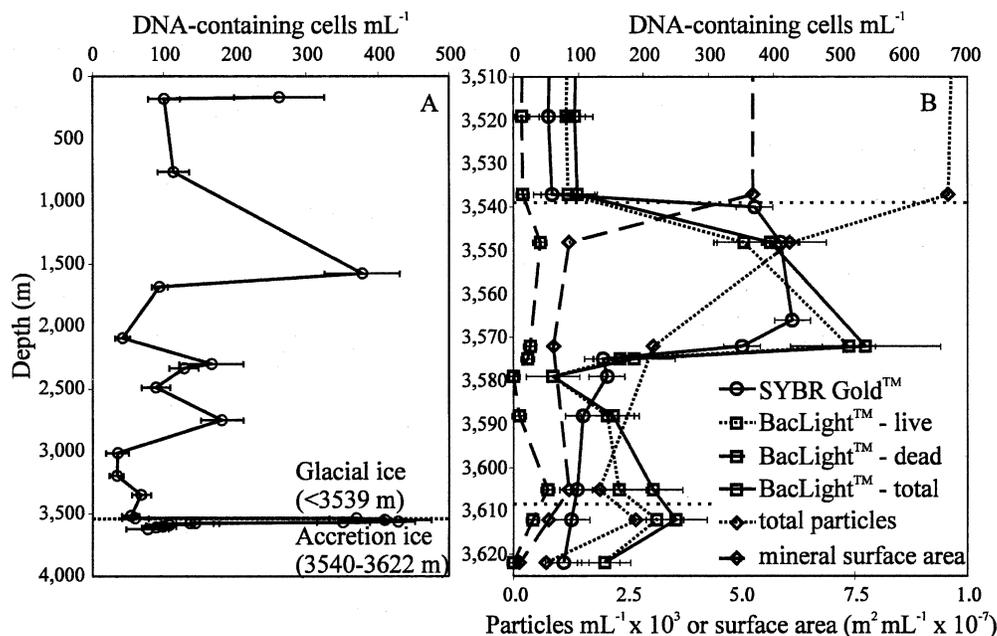
Fig. 2. Concentration of cells with depth in (A) glacial and (B) accretion ice from the Vostok BH5 and 5G ice cores. The data in panel A are from SYBR Gold–stained cell suspensions. Cell staining methods and parameters for particle analysis appear in panel B. Error bars indicate the standard deviation from the cumulative arithmetic mean. The dotted horizontal lines demarcate boundaries between the glacial and accretion ice (3,539 m) and type I and II accretion ice (3,609 m; panel B only).

Table 3. Mineralogy of particles in samples from Vostok ice core determined by EDS. The data represent the mean proportion (%) of the particles for each mineral type from the analysis of 88 meteoric (1,686, 2,758, 2,334, 3,081, and 3,537 m depth) and 75 accreted (3,548, 3,572, 3,605, 3,612, and 3,622 m depth) ice particles.

	Mean proportion (%)	
	Meteoric ice ($n=88$)	Accreted ice ($n=75$)
Albite	9	8
Anorthite	2	4
K-feldspar	14	3
Quartz	28	17
Biotite	19	12
Chlorite	3	1
Iron oxide	2	13
Diopside	1	3
Hornblende	2	3
Gypsum	1	0
Other Fe-containing minerals	11	35
Meteorite	6	1

et al. 2002), data collected on different core sections are not directly comparable. Also, published data on cell density in the accretion ice have used widely differing techniques, ranging from flow cytometry (Karl et al. 1999), SEM (Priscu et al. 1999), fluorescent primary amine stains (fluorescamine; Abyzov et al. 2001), and fluorescent DNA stains (SYBR Gold and BacLight; Christner et al. 2005; this study). Despite these methodological differences, our cell abundance estimates from the accretion ice are within the range reported for samples between 3,541 and 3,611 m (200–3,000 cells mL^{-1}; Karl et al. 1999; Priscu et al. 1999; Abyzov et al. 2001). The most dramatic shift (a greater than sixfold increase) in the density of cells occurred in samples originating from the transition from glacial ice to that formed by the subglacial freezing of lake water to the bottom of the ice sheet (Fig. 2A,B). The density of SYBR Gold–stained cells between 3,540 and 3,572 m (range 350 ± 37 to 430 ± 23 cells mL^{-1}) was significantly higher ($p < 0.001$) than cell densities <3,575 m (range 77 ± 30 to 140 ± 23 cells mL^{-1}). BacLight–stained cells between 3,540 and 3,572 m were also significantly higher ($p = 0.002$) than cell densities <3,575 m. Although SYBR Gold–stained cells decreased with depth <3,575 m (Fig. 2B) and BacLight–stained cells increased over this same depth range, these differences were not statistically significant (paired *t*-test, $p = 0.215$).

Analyses of mineral particles in the glacial ice ($n = 88$) and accretion ice ($n = 75$; Table 3) revealed a mixture of plagioclase feldspars (11% in glacial ice and 12% in accretion ice), potassium feldspars (14% and 3%), quartz (28% and 17%), micas (22% and 13%), and traces of iron oxide (2% and 13%). Other common iron-containing compounds, including Fe-Cr oxide (chromite) and Fe-Ni sulfide particles, were identified in both the glacial ice (11%) and the accretion ice (35%). On the basis of this analysis, the mixture of minerals in the glacial and accretion ice is broadly similar, although the accretion ice

has a higher proportion of oxidized Fe minerals. Although the EDS technique is not sufficient to detect oxidized/reduced forms of Fe, the presence of iron oxide is inferred by significant amounts of both Fe and O in the EDS scans and the relatively high dissolved oxygen levels predicted in the surface of the lake (McKay et al. 2003). The proportion of organic particles (Table 2) in the glacial ice varies from 15% to 40% of the total (by number). The mean proportion of organic particles in the accretion ice was higher than in the glacial ice by both number (46% vs. 29%) and by volume (65% vs. 58%). Ice from 3,539–3,609 m (type I accretion ice) contained mineral particulates ranging from <1 to 45 μm (Royston-Bishop et al. 2005). Some of these particulates were aggregated into larger "inclusions" up to a few millimeters in diameter, as observed by Souchez et al. (2002) and Priscu et al. (1999). The accretion ice <3,572 m contained fewer particles than all glacial ice samples examined. The deepest accretion ice (3,622 m) had the fewest number of total particles of all accretion ice samples (700 particles mL^{-1}; Fig. 2B). The surface area of mineral particles (assumed to be spherical) followed the same trend, with $1.3–4.5 \times 10^{-7}$ m^2 mL^{-1} in the glacial ice and $<1.2 \times 10^{-7}$ m^2 mL^{-1} at <3,572 m. A substantial decrease in mineral particulates at depths >3,610 m (Fig. 2B) corroborates the idea that the ice accreted over a deep part of the water column east of the bedrock ridge that separates the shallow embayment from the main lake (Fig. 1B; Bell et al. 2002).

Our data show the highest levels of particulate matter between 3,540 and 3,572 m (Fig. 2B) in the type I accretion ice, indicating that the shallow embayment contains elevated levels of suspended cells and particles (organic and mineral) relative to surface waters over the deep central portion of the lake's southern basin (Fig. 1B). Royston-Bishop et al. (2005) estimated that particulates (including cells) <23 μm could ascend in the water column, assuming vertical water velocities of 0.0003 m s^{-1}. SEM analysis on accreted ice has shown that bacterial cells are often associated with organic and inorganic particles (Priscu et al. 1999), implying that a portion of the cells within the lake water are not free living. Similar results have been reported for the permanently ice-covered, low–kinetic energy water columns in lakes of the McMurdo Dry Valleys, Antarctica (Lisle and Priscu 2004). On the basis of the stoichiometry of major ions during weathering experiments (Royston-Bishop et al. unpubl. data), particulates released from the accretion ice are involved in chemical weathering reactions (e.g., carbonate dissolution, feldspar hydrolysis, and sulfide oxidation) believed to be similar to those taking place in other subglacial environments (Bottrell and Tranter 2000; Tranter et al. 2002). The soluble ions (e.g., Mg^{2+}, Ca^{2+}, SO$_4^{2-}$) released in these weathering processes could provide microorganisms in the lake with macronutrients and electron acceptors.

Microbial viability and activity—Differential cell staining revealed that the majority (75–99%) of cells in the melted accretion ice are potentially viable (Fig. 2B), which is comparable to the ~80% value reported by Sheridan et al. (2003) from a single depth of "silty" basal ice in the GISP2

Table 4.   Respiration of [^{14}C]glucose to $^{14}CO_2$ in melted samples from Vostok glacial (3,519 m) and accretion ice (3,548, 3,572, 3,603, and 3,612 m). The rates are expressed as the arithmetic mean of replicate samples ($n=5$ or 6) plus or minus the standard deviation.

| | Respiration (nmol L^{-1} d^{-1}) | | | |
| | 10°C | | −3°C* | |
Sample (m)	glucose	carbon	glucose	carbon
3,519	0.98±0.24	0.39±0.10	0.33±0.0082	0.13±0.033
3,548	1.1±0.030	0.44±0.010	0.38±0.011	0.15±0.0050
3,572	0.97±0.29	0.39±0.12	0.33±0.099	0.13±0.040
3,603†	ND	ND	0.80–1.3±1.1	0.32–0.50±0.43
3,612	0.040±0.030	0.020±0.010	0.013±0.0090	0.0050±0.0030

ND, not determined.

* For comparison, metabolic rates were converted to the ambient lake temperature of −3°C (Wüest and Carmack 2000) with the Arrhenius equation, as described in the text.

† Karl et al. (1999).

core (Greenland). The respiration of radiolabeled glucose to $^{14}CO_2$ (Table 4) was detected in four (3,519, 3,548, 3,572, and 3,612 m depth) of the six samples analyzed (samples from 3,605 and 3,622 m did not release measurable $^{14}CO_2$), corroborating the presence of viable heterotrophic cells. Although glucose respiration was measurable in these samples after 20 d of incubation (0.040 ± 0.030 to 1.1 ± 0.030 nmol glucose L^{-1} d^{-1} at 10°C), the radioactivity in the TCA-insoluble fraction (i.e., incorporation of substrate into macromolecules) was not statistically different from time zero kills ($p = 0.18$–0.58). Our enrichment culturing studies on these samples have required up to 6 months of incubation in the dark at 4°C before growth is initiated (Christner and Priscu unpubl. data). After this apparent period of resuscitation, the microbial (bacteria and yeast) species recovered and grew to visible densities on both liquid and agar-solidified media in <10 d, and many of the isolates were capable of growth to the stationary phase in 40 h at 22°C. When nongrowing and sublethally injured cells are placed in a growth situation (e.g., Dodd et al. 1997), metabolism must first be initiated to repair incurred cellular damage before growth and reproduction can occur. Thus, if our incubations had been conducted over a longer time frame, we would have expected such carbon-fed cells to eventually initiate the growth phase.

The metabolic rates from the 10°C incubation were converted to the ambient lake temperature of −3°C (Wüest and Carmack 2000) with the Arrhenius equation and an energy of activation of 12,600 kcal mol^{-1} (empirically determined Q_{10} of 2.3 from bacterial production in a permanently ice-covered Antarctic lake located in the McMurdo Dry Valleys; Takacs and Priscu 1998). With this correction, the respiration rate under ambient lake temperatures is estimated to be 0.013 ± 0.0090 to 0.38 ± 0.011 nmol glucose L^{-1} d^{-1} (or 0.0050 ± 0.0030 to 0.15 ± 0.0050 nmol C L^{-1} d^{-1}), which is on the low end of the range reported by Karl et al. (1999) for an accretion ice core from 3,603 m (0.32–0.50 ± 0.43 nmol C L^{-1} d^{-1} at −3°C). It is important to recognize that our rate calculations assume that the in situ [^{12}C]glucose concentration was insignificant in the melted ice samples and that respiration and incorporation were linear over the entire incubation period.

Molecular phylogenetic analysis—Because of the lack of DNA amplification in all control reactions and identical results from three replications of the experiment with three different primer combinations (i.e., differing sequence and priming position on the small subunit rRNA gene), we conclude that the amplification products generated with the DNA template from the sample from 3,622 m were from authentic amplification events. These PCR amplifications were separated in time and purposely conducted with fresh molecular biological reagents, tubes, and pipette tips. Repeatable PCR results occurred with the use of DNA template from the 3,622-m sample (i.e., in terms of the ability to detect amplifiable DNA), yet the sequence of the clones obtained from nested amplifications with the primers 515F and 1391R or 1492R differed. The exception was the library constructed from nested amplification with the primers 515F and 926R, which contained clones (~400 base pairs) 100% identical to the β or γ phylotypes (Fig. 3). Sequencing and phylogenetic analysis of the 900–1,000 base pair small subunit rRNA gene sequences obtained revealed a low diversity of clones that classify within the β, γ, and δ subdivisions of the phylum *Proteobacteria* (Fig. 3).

The low species diversity in the ice sample from 3,622 m was likely a reflection of the DNA template concentration and the particular method used for PCR amplification. For each PCR reaction, either 10 or 67 μL of meltwater was used without filtration, which on the basis of cell density (Fig. 2A,B), would represent 1–10 DNA-containing cells. It is important to recognize that preserved nucleic acids and those released from lysed cells during melting represent an additional unquantifiable pool of target DNA sequence in these experiments. Operating under such suboptimal amplification conditions limited conclusions regarding the microbial diversity present in the sample, not to mention the actual microbial diversity within Lake Vostok itself. However, the rationale for eliminating conventional DNA extraction protocols was based primarily on minimizing sample exposure to prevent contamination, which is a very relevant concern when conducting sensitive PCR analyses on low DNA–containing samples (e.g., Willerslev et al. 2004).

Realizing the caveats regarding sample size, five of the β-*Proteobacteria* clone sequences were closely related (96–

Desulfuromonas palmitatis (U28172); 83-84%
Geopsychrobacter multivorans (AY579997); 84-85%
Pelobacter massiliensis (AY187308); 82-83%
Pelobacter venetianus (U41562); 83-84%
Pelobacter carbinolicus (U23141); 83-84%
permanently cold marine sediment clone, Svalbard (AJ241001); 83%
anaerobic TCB-transforming consortium clone (AJ009449); 83%
clone from Australian arid-zone soils (AF234131); 94-95%
Vostok clone 3622-10/1391-2 (DQ675592)
Vostok clone 3622-10/1391-5&6 (DQ675593)
Vostok clone 3622-10/1391-1 (DQ675591)

δ

endosymbiont of the tube worm *Ridgeia piscesae* (AY129120); 90%
sulfur-oxidizing bivalve (*Lucina floridana*) symbiont (L25707); 90-91%
sulur-oxidizing bacteria from hydrothermal vent (AF170424); 85%
Thioalkalispira microaerophila (AF481118); 84-85%
Thiobacillus prosperus (AY034139); 89%
Thioalkalivibrio denitrificans (AF126545); 90%
Vostok clone 3622-67/1492-15 (DQ675600)
Vostok clone 3622-67/1492-1 (DQ675599)
Beggiatoa species (L40997); 89-90%
Acidithiobacillus ferrooxidans (AF387301); 91%

γ

Methylobacillus flagellatus (M95651); 96%
Aminomonas aminovorus (AY027801); 96-97%
clone from gas-degrading biofilter (AJ318162); 97%
Vostok clone 3622-67/1391-6 (DQ675596)
Vostok clone 3622-67/1391-10 (DQ675598)
Vostok clone 3622-67/1391-1&9 (DQ675594)
Vostok clone 3622-67/1391-7 (DQ675597)
Vostok clone 3622-67/1391-2 (DQ675592)
clone from gas-degrading biofilter (AJ318113); 96-97%
Methylophilus methylotrophus (L15475); 96%
Methylophilus freyburgensis (AJ517772); 96%
Methylophilus leisingerii (AF250333); 95%
picoplankton clone, Cape Hatteras (U70704); 94-95%

β

0.10

To outgroups

Methylobacterium extorquens

Fig. 3. Phylogenetic analysis of β, γ, and δ proteobacterial small subunit rRNA sequences amplified from DNA in the 3,622-m Vostok accretion ice sample. The sequences obtained were aligned on the basis of secondary structure (Ludwig et al. 2004), and an 820-nucleotide mask (552–1,370, *E. coli* 16S rRNA gene numbering) of unambiguously aligned positions was constructed. Clones are in bold font and designated by the depth of recovery, the concentration of meltwater added to each initial PCR reaction, the reverse primer used for amplification, and the clone number (i.e., Vostok clone 3622-10/1391-1 is clone No. 1 amplified from sample recovered at 3,622 m with the use of 10 μL of meltwater for the template and the small subunit rRNA nucleotide primers 515F and 1391R). GenBank accession numbers are listed in parentheses, followed by percent identity to the nearest Vostok clone. The maximum likelihood tree was generated by fastDNAml (Olsen et al. 1994), and the scale bar indicates 0.1 fixed substitutions per nucleotide position. The 16S rRNA gene sequences of *Aquifex pyrophilus* and *Methanobacterium thermoautotrophicum* were used as outgroups.

97%; identity of 823 aligned nucleotides) to aerobic methylotrophic species in the genera *Methylobacillus* (Urakami and Komagata 1986) and *Methylophilus* (Jenkins et al. 1987). The type I methylotrophs are a phylogenetic group in which substrate use is restricted to C-1 compounds (e.g., methanol, formate, and carbon monoxide) and carbon assimilation is via the ribulose monophosphate pathway (Brusseau et al. 1994). Molecular-based oceanographic surveys indicate that *Methylobacillus*- and *Methylophilus*-related phylotypes are more abundant in coastal sites than in the open ocean (Rappé et al. 2000), but no systematic ecological studies of these species have been reported. Christner et al. (2001) recovered a facultative methylotrophic α-*Proteobacteria* isolate from accretion ice

at 3,593 m, supporting the notion that microbial niches for methylotrophy could exist in the lake.

Polyphasic data sets infer that a small subunit rRNA gene identity >97% correlates with a species-level phylogenetic relationship (Stackebrandt and Goebel 1994). Taking the 97% identity value as a taxonomic approximation for assessing molecular sequence data, neither the γ nor the δ proteobacterial clones (Fig. 3) are related at the species level to previously encountered environmental sequences or cultivated isolates. However, the phylotypes do cluster with bacterial species that collectively share common and interesting metabolic capabilities. The nearest phylogenetic neighbors (90–91%; identity of 933 aligned nucleotides) of the two cloned γ-*Proteobacteria* sequences

are (1) *Acidithiobacillus ferrooxidans*, an acidophilic che-molithoautotroph that oxidizes ferrous iron (Kelly and Wood 2000) or can use H_2/Fe^{3+}, H_2/S^0, or S^0/Fe^{3+} anaerobically for energy generation (Ohmura et al. 2002), and (2) a cloned sequence from a sulfur-oxidizing chemoautotrophic endosymbiont of the bivalve host *Lucina floridana* (Distel et al. 1994). The δ-Proteobacteria small subunit rRNA gene sequences have 94–95% identity (822 aligned nucleotides) to a clone recovered from Australian arid-zone soils and are distantly related (82–85%) to members of the genera *Desulfuromonas, Geopsychrobacter*, and *Pelobacter*. With the exception of the *Myxococcales* and *Bdellovibrionaceae* (obligately aerobic species that prey on other bacteria), all other characterized species of the δ-Proteobacteria are strict anaerobes that respire via the reduction of electron acceptors such as SO_4^{2-}, S°, Fe(III), and Mn(IV) (e.g., Lovely et al. 1995). Considering that metabolic inferences for the γ and δ proteobacterial clones are based on distant phylogenetic relationships, confident predictions about physiology are unachievable. Although equivocal, the clustering of the identified small subunit rRNA gene sequences among aerobic and anaerobic species of bacteria with metabolisms dedicated to iron and sulfur respiration or oxidation implies that these metals play a role in the bioenergetics of microorganisms that occur in Lake Vostok.

Biogeochemical conditions in Lake Vostok—Multisample (Table 1) analysis of the 5G core revealed that the concentration of NPOC in the glacial ice ranged from 2 to 80 μmol L^{-1} (Fig. 4A), with the largest value in the entire core (100 μmol L^{-1}) obtained at 3,605 m in a deep section of the type I accretion ice (Fig. 4B). The total amino acid concentration (i.e., DFAAs + DCAAs + protein) in the accretion ice (Fig. 4A,B) ranged from 0.01% to 2% of the NPOC pool. Amino acids represented 0.6–2% of the NPOC fraction in glacial ice, with a maximum of 20% in a sample from 2,303 m (Fig. 4A). Although the correlation between NPOC and the amino acid concentration in the accretion ice was significant ($r = 0.83$, $p < 0.02$; Fig. 4C), no significant relationship existed between these parameters in the glacial ice ($r = 0.015$, $p < 0.03$).

A detailed geochemical study by de Angelis et al. (2004) of Lake Vostok accretion ice from 3,538 to 3,619 m revealed large vertical variation in the concentration of major ions, which have been verified by our own analysis (Fig. 5). Sodium, K^+, Ca^{2+}, Mg^{2+}, Cl^-, and SO_4^{2-} concentrations vary considerably in type I accretion ice and often exceeded those in the glacial ice by two to three orders of magnitude. Type II accretion ice more closely resembled the glacial ice but is, on average, less concentrated (Table 5; Fig. 5). The concentrations of NO_3^- (de Angelis et al. 2004) and SO_4^{2-} peak in the type I accretion ice and decreased with increasing depth, similar to the profile at the oxic–anoxic interface in a typical aquatic water column. However, the accretion ice depth profile records horizontal and not vertical trends in the lake water column; therefore, the inferred gradient would exist in surface waters between the shoreline and main body of
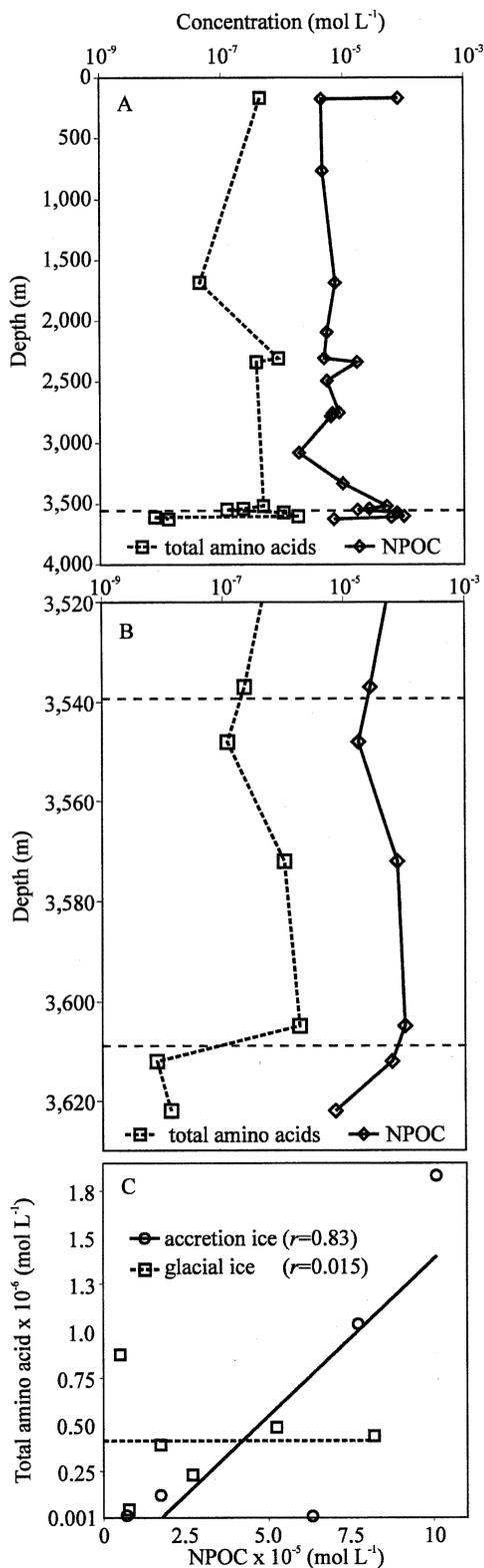
Fig. 4. Nonpurgeable organic carbon (NPOC) and total amino acid concentrations in the Vostok ice core. Values are given for (A) the entire ice core depth range and (B) a high-resolution profile in the accretion ice. (C) The relationship between NPOC and the amino acid concentration in glacial and accretion ice. In panels A and B the dotted horizontal lines demarcate boundaries between the glacial and accretion ice (3,539 m) and type I and II accretion ice (3,609 m; panel B only).
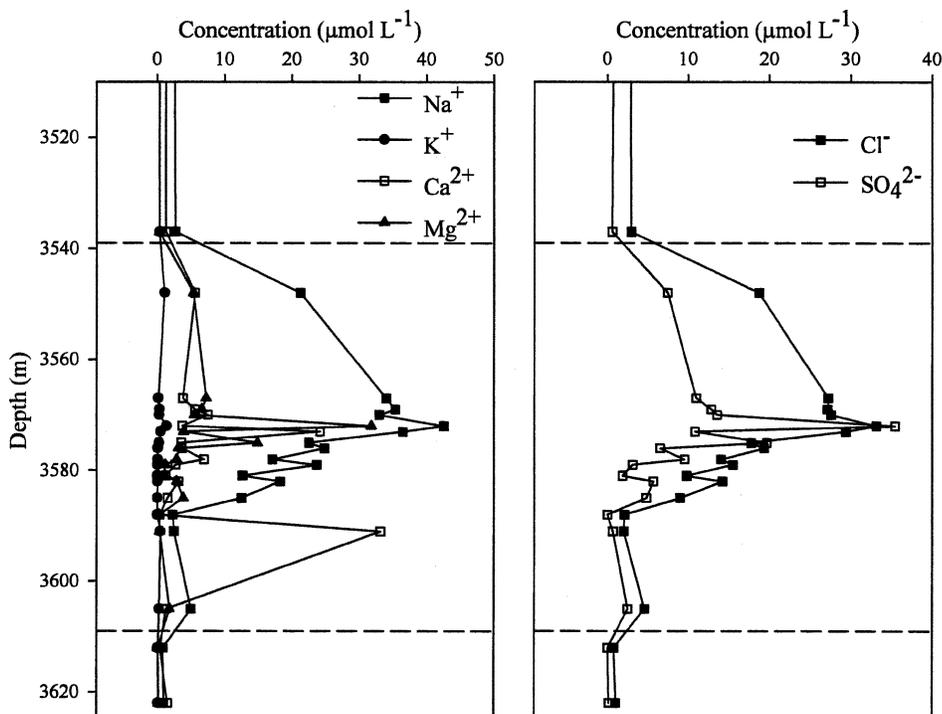
Fig. 5. Major ion concentrations in the deep glacial and accretion ice of the Vostok 5G borehole determined by ion chromatography. Dotted lines demarcate boundaries between the glacial and accretion ice (3,539 m) and type I and II accretion ice (3,609 m).

Lake Vostok. Siegert et al. (2003) contend that even with a constant supply of oxygen (i.e., from melting glacial ice and air hydrate dissolution), portions of the lake and the deep sediments might be anoxic if sulfide oxidation (i.e., abiotic weathering of rock flour), microbial respiration, or both are consuming dissolved O_2. Our data imply that potential biotic and sulfide sinks of O_2 (Fig. 2B) are more abundant in shallow depths near the western coastline of Lake Vostok (Fig. 1B).

The concentration of total dissolved solids (TDS) in the lake water was estimated by applying ice–water partition coefficients to the major ion concentrations in the accretion ice. A partition coefficient describes the ratio of the concentration of a particular solute in ice relative to that in the source water for the ice. Because solutes and cells are excluded from the lattice when ice forms (e.g., Killawee et al. 1998), coefficients are always <1. Assuming that the ice–water partition coefficients are the same as those calculated from the permanent ice cover and water column of Lake Bonney in the McMurdo Dry Valleys, we estimate TDS concentrations of water in the embayment (from type I accretion ice) and the main lake (from type II accretion ice) of 34 and 1.5 mmol L^{-1}, respectively (Table 5). The estimated TDS of the embayment is higher than all previous predictions from type I accretion ice (<16 mmol L^{-1}; Jouzel et al. 1999; Priscu et al. 1999, Siegert et al. 2003) but significantly fresher than seawater, which has a TDS of ~700 mmol L^{-1} (Garrels and Christ 1965). Our predicted TDS values classify the near-surface waters of Lake Vostok as a low-salinity soft water lake (Wetzel 2001). Estimates of salt saturations (from

PHREEQC, U.S. Geological Survey, available at http://wwwbrr.cr.usgs.gov/projects/GWC_coupled/phreeqc/index.html) for the most concentrated lake water in the embayment (back-calculated from the most concentrated type I accretion ice sample) imply that the surface lake waters are almost saturated with common minerals such as aragonite ($CaCO_3$) and anhydrite ($CaSO_4$). These estimates are based on the assumption that the pH is ~6.0 (the pH of the accretion ice) and that the charge imbalance is accounted for by HCO_3^-. It is important to note that our estimates represent the near-surface waters of Lake Vostok because the accretion ice is only formed from surface waters. It is possible that the ionic strength will be higher with depth, as observed in the permanently ice-covered Lakes Vanda and Bonney in the McMurdo Dry Valleys (Spigel and Priscu 1998).

The use of NPOC concentrations from the accretion ice (Fig. 4A,B) in concert with a partition coefficient calculated from Lake Bonney (0.40; Table 5) leads to predictions of NPOC concentrations in the lake ranging from 17 to 250 μmol L^{-1}. These values are in the range of those reported by Priscu et al. (1999) and Karl et al. (1999) on the basis of data from ice cores from 3,590 m (100 μmol L^{-1}) and 3,603 m (18 μmol L^{-1}), respectively. Accretion rates in the lakes of the McMurdo Dry Valleys (~30 cm yr^{-1}; Adams et al. 1998) are an order of magnitude higher than those in the Lake Vostok system (~4 cm yr^{-1}; Bell et al. 2002). In theory, higher freezing rates should increase the partition coefficient (Killawee et al. 1998); therefore, our extrapolations to actual lake concentrations of NPOC should be viewed as an underestimate. Acid-extractable

Table 5. NPOC, biomass, and major ion concentrations in glacial ice and accretion ice from the Vostok 5G borehole. Predicted concentrations for lake water were derived as described in the text.

Constituent	NPOC (μmol L^{-1})	Biomass (cells mL^{-1})	Concentration (μmol L^{-1})						Total dissolved solids (mmol L^{-1})
			Na$^+$	K$^+$	Ca^{2+}	Mg^{2+}	Cl$^-$	SO$_4^{2-}$	
Glacial ice (average)	16	120	2.4	0.40	1.09	0.36	2.8	1.8	0.0088
Type I accretion ice (average)	65	260	22	0.32	6.8	5.8	17	9.1	0.061
Type II accretion ice (average)	35	83	0.92	0.13	0.98	0.15	0.94	0.15	0.0033
Embayment water*†	160	460	10,000	14	2,600	2,700	7,300	11,000	34
Main lake water†‡	86	150	430	5.9	370	69	400	180	1.5
Average continental rainfall§	NA	NA	26	7.7	52	11	31	21	0.15
Average marine/ coastal rainfall§	NA	NA	130	10	21	39	160	21	0.38
Average surface seawater	40–80‖	0.05–5×10⁵¶	48,000#	10,000#	10,000#	54,000#	560,000#	28,000#	710

NA, not available.

* Prediction on the basis of average type I accretion ice composition.

† Partitioning coefficients for NPOC, biomass, Na$^+$, K$^+$, Ca^{2+}, Mg^{2+}, Cl$^-$, and SO$_4^{2-}$ are 0.40, 0.56, 0.0021, 0.022, 0.0026, 0.0022, 0.0023, and 0.00083, respectively.

‡ Prediction on the basis of average type II accretion ice composition.

§ Wetzel (2001).

‖ Williams (1975), Hansell and Carlson (2001), Sharp et al. (2002).

¶ Whitman et al. (1998).

Garrels and Christ (1965).

amino acids have been shown to represent a significant fraction of the bioavailable NPOC in lake and ocean ecosystems (Weiss and Simon 1999; Rosenstock and Simon 2001). The acid-extractable amino acid concentration from core depths between 3,539 and 3,622 m mirrored the NPOC concentration (Fig. 4B) and indicates that ≤2% of the NPOC in Lake Vostok is composed of acid-extractable amino acids. DFAAs represent 1–10% of the acid-extractable amino acids in type I accretion ice, whereas the entire amino acid pool exists as DFAAs in the type II accretion ice. The NPOC and total acid-extractable amino acid concentration both peaked at the transition between type I and II accretion ice (3,572–3,612 m; Fig. 4B), a portion of the ice core representing lake water frozen at the transition from the shallow embayment to the eastern portion of the lake proper (Bell et al. 2002). These data indicate that the near shoreline represents a source for amino acids and, together with the cell density data, imply that this region has elevated rates of heterotrophic biological activity and associated amino acid transformations relative to the main body of the lake.

Bioenergetics in Lake Vostok—Biogeochemical and microbiological trends observed in the accretion ice allowed us to define several ecological scenarios that would support a viable ecosystem in Lake Vostok. First, organic carbon originating from the sediments or the overlying ice sheet could support an exclusively heterotrophic community. We measured rates of aerobic respiration in cells from type I and II accretion ice (Table 4), substantiating previously documented reports of viable heterotrophic bacteria in these samples (Karl et al. 1999; Christner et al. 2001). From cell partitioning coefficients calculated for accretion ice (see discussion above) and the cell densities determined for accretion ice in this study, we estimate the near-surface lake water to have between 140 and 770 cells mL^{-1} (partitioning coefficient of 0.56; Table 5). Assuming that the lake is in a hydraulic steady state (i.e., glacial ice melt in the north is balanced by water removed as accretion ice in the south; Bell et al. 2002), we computed source and sink estimates for NPOC. Given a basal melt volume of 0.15 km³ yr^{-1} (estimated from the lake area and accretion rate in Bell et al. [2002]), the lake would be supplied with 0.034–1.4 × 10⁵ g NPOC yr^{-1} from the overlying glacial ice sheet (i.e., g NPOC L^{-1} in glacial ice × L yr^{-1} of glacial ice melt = g NPOC yr^{-1} of source). Our measurements on the accretion ice, in concert with the estimated accretion rate of 0.15 km³ yr^{-1} (Bell et al. 2002), infer that 0.085–1.3 ×

10^3 g NPOC yr^{-1} are removed from the lake via the accretion ice. From these data and a residence time for the lake of 40,000 yr (Bell et al. 2002; Studinger et al. 2004), NPOC would accumulate in the lake over a single residence period, reaching levels between 15 and 640 nmol NPOC L^{-1}. After ~375 residence times (i.e., if the lake is at least 1.5×10^7 yr old; Siegert et al. 2003), the NPOC concentration would range from 6 to 240 μmol NPOC L^{-1}, which is similar to the range we calculated (17–250 μmol NPOC L^{-1}) from our direct measurements of the accretion ice NPOC concentration (Table 5). From the rate of NPOC input, predicted cell numbers in the lake (Table 5), and a cell carbon estimate of 10 fg C cell^{-1} (Christian and Karl 1994) and assuming no abiotic sinks for NPOC in the lake, the positive NPOC flux would provide heterotrophic bacteria with 0.49–3.8 × 10^{-4} g NPOC (g cell C)$^{-1}$ h^{-1}. Thus, even if all the dissolved organic carbon input from the glacial ice was suitable as heterotrophic substrate, it could not provide the carbon demand required for reproductive growth of the entire community (theoretical carbon demand of ~10^{-2} g C [g cell C]$^{-1}$ h^{-1} at -3°C; Price and Sowers 2004); bacterial production in the Ross Sea (Antarctica) at -1°C is 5 × 10^{-2} g C (g cell C)$^{-1}$ h^{-1} (Ducklow 2000), but it would be adequate for maintenance metabolism with no net carbon loss or gain (Price and Sowers 2004). Our calculations should be viewed as conservative because we do not know the ratio of autotrophic to heterotrophic cells in the accretion ice, and it is difficult to constrain the pool of organic carbon from preglacial soil in the lakebed and that transported by glacial scour into the lake. In general, our data and related calculations imply that the lake is ultraoligotrophic, with a total NPOC pool of <250 μmol L^{-1}.

A second possibility for sustaining life in the lake is the existence of a supplemental microbial food web based on chemolithotrophic primary production. Jean-Baptiste et al. (2001) concluded that the ^{3}He:^{4}He ratios within the accretion ice preclude significant hydrothermal input into the lake. However, Bulat et al. (2004) provide an alternative interpretation of this data, suggesting instead that it indicates that fault vents are present in the shallow embayment of the lake, further arguing that a history of long-term tectonic activity in the region and the "oxygen shift" in the accretion ice (resulting from ^{18}O-enriched water produced by weathering at high temperatures) is also consistent with geothermal activity. Although the notion of such possibilities is exciting and implies that a unique subsurface microbial community might exist, a chemolithotrophic-based ecosystem is plausible in the lake without the need to invoke geothermal activity. A range of reduced compounds (e.g., HS$^-$, S^0, and Fe^{2+}; *see* Siegert et al. [2003] for a comprehensive inventory) are predicted to be available to fuel biogeochemical reactions in the lake. Oxidants are supplied by the ice sheet (O$_2$ and NO$_3^-$) and also through the chemical weathering of bedrock and sediment (e.g., SO$_4^{2-}$ from sulfide oxidation). The oxidation of metal sulfides in glacial flour, first employing oxygen and then NO$_3^-$ or Fe^{3+} as electron acceptors, are microbially mediated chemical weathering reactions that have been documented in suboxic and anoxic glacial bed environments (Bottrell and Tranter 2000; Tranter et al. 2002).

Basal ice continually melts into Lake Vostok, introducing glacial debris that contains crushed sulfide and iron minerals in addition to organic material from the bedrock. This input provides the potential for bioenergetic pathways that include sulfide, iron, and manganese oxidation, nitrification, S^0 and SO$_4^{2-}$ reduction, acetogenesis, and methanogenesis (Siegert et al. 2003). Several of the small subunit rRNA gene sequences recovered (Fig. 3) in our study are most closely related to species with metabolic lifestyles involved in metal respiration or oxidation, consistent with microbial energy-generating strategies identified as common in other subglacial environments (Bottrell and Tranter 2000; Tranter et al. 2002; Wadham et al. 2004). A key point about the latter mechanism of sustaining a chemolithotrophic-based ecosystem is that apart from viable inocula, known glacial processes supply the energy source and geothermal inputs to fuel microbial activity within the lake environment are not necessary.

Investigations on the accretion ice recovered from the Vostok ice core have provided valuable data to examine the limnological conditions in Lake Vostok, a large subglacial lake. Our results corroborate the emerging view of Lake Vostok as an ecosystem supporting viable microbial life (i.e., Karl et al. 1999; Priscu et al. 1999; Christner et al. 2001), despite long-term direct isolation from the atmosphere and complete lack of sunlight. The biogeochemical variation we have documented in the accretion ice indicates that conditions have not been uniform in the lake's surface waters either spatially or temporally (i.e., 3–5 × 10^3 yr B.P.; Table 1). One possible explanation for these trends is that biological activity is elevated in the shallow coastline waters relative to surface waters over deeper regions of the lake. Given the enormous logistic effort that will be required to sample the lake cleanly (e.g., Inman 2005), our data provide important background information on the chemical and biological conditions expected near Lake Vostok's western shoreline and in surface waters of the southern basin.

References

ABYZOV, S. S., I. N. MITSKEVICH, M. N. POGLAZOVA, AND OTHERS. 2001. Microflora in the basal strata at Antarctic ice core above the Vostok Lake. Adv. Space Res. **28:** 701–706.

ADAMS, E. E., J. C. PRISCU, C. H. FRITSEN, S. R. SMITH, AND S. L. BRACKMAN. 1998. Permanent ice covers of the McMurdo Dry Valley Lakes, Antarctica: Bubble formation and metamorphism, v. 72, p. 281–295. *In* J. C. Priscu [ed.], Ecosystem dynamics in a polar Desert: The McMurdo Dry Valleys, Antarctica. Antarctic Research Series, American Geophysical Union.

BELL, R. E., M. STUDINGER, A. A. TIKKU, G. K. C. CLARKE, M. M. GUTNER, AND C. MEERTENS. 2002. Origin and fate of Lake Vostok water frozen to the base of the East Antarctic ice sheet. Nature **416:** 307–310.

BOTTRELL, S., AND M. TRANTER. 2000. Sulphide oxidation under partially anoxic conditions at the bed of Haut Glacier d'Arolla, Switzerland. Hydrol. Process. **16:** 2363–2368.

BRUSSEAU, G. A., E. S. BULYGINA, AND R. S. HANSON. 1994. Phylogenetic analysis and development of probes for differentiating methylotrophic bacteria. Appl. Environ. Microbiol. **60:** 626–636.

BULAT, S. A., I. A. ALEKHINA, M. BLOT, AND OTHERS. 2004. DNA signature of thermophilic bacteria from the aged accretion ice of Lake Vostok, Antarctica: Implications for searching for life in extreme icy environments. Intern. J. Astrobiol. **3:** 1–12.

CHRISTIAN, J. R., AND D. M. KARL. 1994. Microbial community structure at the U.S.–Joint Global Ocean Flux Study Station ALOHA: Inverse methods for estimating biochemical indicator ratios. J. Geophys. Res. **99:** 14269–14276.

CHRISTNER, B. C., J. A. MIKUCKI, C. M. FOREMAN, J. DENSON, AND J. C. PRISCU. 2005. Glacial ice cores: A model system for developing extraterrestrial decontamination protocols. Icarus **174:** 572–584.

———, E. MOSLEY-THOMPSON, L. G. THOMPSON, AND J. N. REEVE. 2001. Isolation of bacteria and 16S rDNAs from Lake Vostok accretion ice. Environ. Microbiol. **3:** 570–577.

DE ANGELIS, M., J.-R. PETIT, J. SAVARINO, R. SOUCHES, AND M. H. THIEMENS. 2004. Contributions of an ancient evaporitic-type reservoir to subglacial Lake Vostok chemistry. Earth Planet. Sci. Lett. **222:** 751–765.

DISTEL, D. L., H. FELBECK, AND C. M. CAVANAUGH. 1994. Evidence for phylogenetic congruence among sulfur-oxidizing chemoautotrophic bacterial endosymbionts and their bivalve hosts. J. Mol. Evol. **38:** 533–542.

DODD, C. E. R., R. L. SHARMAN, S. F. BLOOMFIELD, I. R. BOOTH, AND G. S. A. B. STEWART. 1997. Inimical processes: Bacterial self-destruction and sub-lethal injury. Trends Food Sci. Technol. **8:** 238–241.

DUCKLOW, H. 2000. Bacterial production and biomass in the oceans, p. 85–120. *In* D. L. Kirchman [ed.], Microbial ecology of the oceans. Wiley.

GARRELS, R. M., AND C. L. CHRIST. 1965. Solutions, minerals, and equilibria. Freeman Cooper.

GOW, A. J., AND D. A. MEESE. 1996. Nature of basal debris in the GISP2 and Byrd ice cores and its relevance to bed processes. Ann. Glaciol. **22:** 134–140.

HANSELL, D. A., AND C. A. CARLSON. 2001. Dissolved organic carbon in the upper ocean of the central equatorial Pacific Ocean, 1992: Daily and finescale vertical variations. Oceanography **14:** 41–49.

INMAN, M. 2005. The plan to unlock Lake Vostok. Science **310:** 611–612.

JEAN-BAPTISTE, P., J. P. PETIT, V. Y. LIPENKOV, D. RAYNAUD, AND N. I. BARKOV. 2001. Constraints on hydrothermal processes and water exchange in Lake Vostok from helium isotopes. Nature **411:** 460–462.

JENKINS, O., D. BYROM, AND D. JONES. 1987. Methylophilus: A new genus of methanol-utilizing bacteria. Int. J. Syst. Bacteriol. **37:** 446–448.

JOUZEL, J., J. R. PETIT, R. SOUCHEZ, AND OTHERS. 1999. More than 200 meters of lake ice above subglacial Lake Vostok, Antarctica. Science **286:** 2138–2141.

KAPITSA, A. P., J. K. RIDLEY, G. DE Q. ROBIN, M. J. SIEGERT, AND I. A. ZOTIKOV. 1996. A large deep freshwater lake beneath the ice of central East Antarctica. Nature **381:** 684–686.

KARL, D. M., BIRD D. F., K. BJÖRKMAN, T. HOULIHAN, R. SHACKELFORD, AND L. TUPAS. 1999. Microorganisms in the accreted ice of Lake Vostok, Antarctica. Science **286:** 2144–2147.

KELLY, D. P., AND A. P. WOOD. 2000. Reclassification of some species of *Thiobacillus* to the newly designated genera *Acidithiobacillus* gen. nov., *Halothiobacillus* gen. nov. and *Thermithiobacillus* gen. nov. Int. J. Syst. Evol. Microbiol. **50:** 511–516.

KILLAWEE, J. A., I. J. FAIRCHILD, J. L. TISON, L. JANSSENS, AND R. LORRAIN. 1998. Segregation of solutes and gases in experimental freezing of dilute solutions: Implications for natural glacial systems. Geochim Cosmochim Acta **62:** 3637–3655.

LANE, D. J. 1991. 16S/23S rRNA sequencing, p. 115–175. *In* E. Stakebrandt and M. Goodfellow [eds.], Nucleic acid techniques in bacterial systematics. Wiley.

LISLE, J. T., AND J. C. PRISCU. 2004. The occurrence of lysogenic bacteria and microbial aggregates in the lakes of the McMurdo Dry Valleys, Antarctica. Microb. Ecol. **47:** 427–439.

LOVLEY, D. R., E. J. P. PHILLIPS, D. J. LONERGAN, AND P. K. WIDMAN. 1995. Fe(III) and S^0 Reduction by *Pelobacter carbinolicus*. Appl. Environ. Microbiol. **61:** 2132–2138.

LUDWIG, W., O. STRUNK, R. WESTRAM, AND OTHERS. 2004. ARB: A software environment for sequence data. Nucleic Acids Res. **32:** 1363–1371. [doi: 10.1093/nar/gkh293]

MCKAY, C. P., K. P. HAND, P. T. DORAN, D. T. ANDERSON, AND J. P. PRISCU. 2003. Clathrate formation and the fate of noble and biologically useful gases in Lake Vostok, Antarctica. Geophys. Res. Lett. **30,** 1702. [doi:10.1029/2003GL017490]

OHMURA, N., K. SASAKI, N. MATSUMOTO, AND H. SAIKI. 2002. Anaerobic respiration using Fe^{3+}, S^0, and H_2 in the chemolithoautotrophic bacterium *Acidithiobacillus ferrooxidans*. J. Bacteriol. **184:** 2081–2087.

OLSEN, G. J., J. H. NATUSDA, R. HAGSTROM, AND R. OVERBEEK. 1994. fastDNAml: A tool for construction of phylogenetic trees of DNA sequences using maximum likelihood. Comput. Appl. Biosci. **108:** 41–48.

PETIT, J. R., J. JOUZEL, D. RAYNAUD, AND OTHERS. 1999. Climate and atmospheric history of the past 420,000 years from the Vostok ice core, Antarctica. Nature **399:** 429–436.

PRICE, B. P., AND T. SOWERS. 2004. Temperature dependence of metabolic rates for microbial growth, maintenance, and survival. Proc. Natl. Acad. Sci. USA **101:** 4631–4636.

PRISCU, J. C., E. E. ADAMS, W. B. LYONS, AND OTHERS. 1999. Geomicrobiology of subglacial ice above Lake Vostok, Antarctica. Science **286:** 2141–2144.

———, R. E. BELL, S. A. BULAT, AND OTHERS. 2003. An international plan for Antarctic subglacial lake exploration. Polar Geogr **27:** 69–83.

RAPPÉ, M. S., K. L. VERGIN, AND S. J. GIOVANNONI. 2000. Phylogenetic comparisons of a coastal bacterioplankton community with its counterparts in open ocean and freshwater systems. FEMS Microbiol. Ecol. **33:** 219–232.

REYSENBACH, A.-L., AND N. R. PACE. 1995. Reliable amplification of hyperthermophilic archaeal 16S rRNA genes by the polymerase chain reaction. *In* F. T. Robb and A. R. Place [eds.], Archaea: A laboratory manual. Cold Spring Harbor Laboratory, Cold Spring Harbor Press.

RIDLEY, J. K., W. CUDLIP, AND S. W. LAXON. 1993. Identification of subglacial lakes using ERS-1 radar altimeter. J. Glaciol. **39:** 625–634.

ROBIN, G. DE Q., D. J. DREWRY, AND D. T. MELDRUM. 1977. International studies of ice sheet and bedrock. Philos. Trans. R. Soc. Lond **279:** 185–196.

ROSENSTOCK, B., AND M. SIMON. 2001. Sources and sinks of dissolved free amino acids and protein in a large and deep mesotrophic lake. Limnol. Oceanogr. **46:** 644–654.

ROYSTON-BISHOP, G., J. C. PRISCU, M. TRANTER, B. C. CHRISTNER, M. J. SIEGERT, AND V. LEE. 2005. Incorporation of particulates into accreted ice above subglacial Lake Vostok, Antarctica. Ann. Glaciol. **40:** 145–150.

SHARP, J. H., C. A. CARLSON, E. T. PELTZER, D. M. CASTLE-WARD, K. B. SAVIDGE, AND K. R. RINKER. 2002. Final dissolved organic carbon broad community intercalibration and preliminary use of DOC reference materials. Mar. Chem. **77:** 239–253.

SHARP, M., J. PARKES, B. CRAGG, I. J. FAIRCHILD, H. LAMB, AND M. TRANTER. 1999. Widespread bacterial populations at glacier beds and their relationship to rock weathering and carbon cycling. Geology **27:** 107–110.

SHERIDAN, P. P., V. I. MITEVA, AND J. E. BRENCHLEY. 2003. Phylogenetic analysis of anaerobic psychrophilic enrichment cultures obtained from a Greenland glacier ice core. Appl. Environ. Microbiol. **69:** 2153–2160.

SIEGERT, M. J., S. CARTER, I. TABACCO, S. POPOV, AND D. D. BLANKENSHIP. 2005. A revised inventory of Antarctic subglacial lakes. Antarct. Sci. **17:** 453–460.

———, R. KWOK, C. MAYER, AND B. HUBBARD. 2000. Water exchange between the subglacial Lake Vostok and the overlying ice sheet. Nature **403:** 643–646.

———, M. TRANTER, J. C. ELLIS-EVANS, J. C. PRISCU, AND W. B. LYONS. 2003. The hydrochemistry of Lake Vostok and the potential for life in Antarctic subglacial lakes. Hydrol. Process. **17:** 795–814.

SIMÕES, J. C., J. R. PETIT, R. SOUCHEZ, AND OTHERS. 2002. Evidence of glacial flour in the deepest 89 m of the Vostok ice core. Ann. Glaciol. **35:** 340–346.

SOUCHEZ, R., P. JEAN-BAPTISTE, J. R. PETIT, V. Y. LIPENKOV, AND J. JOUZEL. 2002. What is the deepest part of the Vostok ice core telling us? Earth Sci Rev. **60:** 131–146.

SPIGEL, R. H., AND J. C. PRISCU. 1998. Evolution of temperature and salt structure of L. Bonney, a chemically stratified Antarctic lake. Hydrobiologia **321:** 177–190.

STACKEBRANDT, E., AND B. M. GOEBEL. 1994. Taxonomic note: A place for DNA–DNA reassociation and 16S rRNA sequence analysis in the present species definition in bacteriology. Int. J. System. Bacteriol. **44:** 846–849.

STUDINGER, M., R. E. BELL, G. D. KARNER, AND OTHERS. 2003. Ice cover, landscape setting, and geological framework of Lake Vostok, East Antarctic. Earth Planet. Sci. Lett. **205:** 195–210.

———, ———, AND A. A. TIKKU. 2004. Estimating the depth and shape of subglacial Lake Vostok's water cavity from aerogravity data. Geophys. Res. Lett. **31**, L12401. [doi:10.1029/2004GL019801]

SWOFFORD, D. L. 1999. PAUP*. Phylogenetic Analysis Using Parsimony (*and Other Methods). Version beta 4a. Sinauer Associates, Sunderland, Massachusetts.

TAKACS, C. T., AND J. C. PRISCU. 1998. Bacterioplankton dynamics in the McMurdo Dry Valley Lakes: Production and biomass loss over four seasons. Microb. Ecol. **36:** 239–250.

TRANTER, M., M. J. SHARP, H. R. LAMB, G. H. BROWN, B. P. HUBBARD, AND I. C. WILLIS. 2002. Geochemical weathering at the bed of Haut Glacier d'Arolla, Switzerland—a new model. Hydrol. Process. **16:** 959–993.

URAKAMI, T., AND K. KOMAGATA. 1986. Emendation of *Methylobacillus* Yordy and Weaver 1977, a genus for methanol-utilizing bacteria. Int. J. Syst. Bacteriol. **36:** 502–511.

WADHAM, J. L., S. BOTTRELL, M. TRANTER, AND R. RAISWELL. 2004. Stable isotope evidence for microbial sulphate reduction at the bed of a polythermal high Arctic glacier. Earth Planet. Sci. Lett. **219:** 341–355.

WEISS, M., AND M. SIMON. 1999. Consumption of labile dissolved organic matter by limnetic bacterioplankton: The relative significance of amino acids and carbohydrates. Aquat. Microb. Ecol. **17:** 1–12.

WELCH, K. A., W. B. LYONS, E. GRAHAM, K. NEUMANN, J. M. THOMAS, AND D. MIKESELL. 1996. Determination of major element chemistry in terrestrial waters from Antarctica by ion chromatography. J. Chromatogr. A **739:** 257–263.

WETZEL, R. G. 2001. Limnology, lake and river ecosystems. Academic, available at http://wwwbrr.cr.usgs.gov/projects/GWC_coupled/phreeqc/index.html

WHITMAN, W. B., D. C. COLEMAN, AND W. J. WIEBE. 1998. Prokaryotes: The unseen majority. Proc. Natl. Acad. Sci. USA **95:** 6578–6583.

WILLERSLEV, E. A., A. J. HANSEN, AND H. N. POINAR. 2004. Isolation of nucleic acids and cultures from fossil ice and permafrost. Trends Ecol. Evol. **19:** 141–147.

WILLIAMS, P. J. 1975. Biological and chemical dissolved organic material in seawater, p. 301–364. *In* J. P. Riley and G. Skirow [eds.], Chemical oceanography, v. 2, 2nd ed. Academic.

WÜEST, A., AND E. CARMACK. 2000. A priori estimates of mixing and circulation in the hard-to-reach water body of Lake Vostok. Ocean Model. **2:** 29–43.